Journal of Alloys and Compounds 509 (2011) 1163–1171

Contents lists available at ScienceDirect

Journal of Alloys and Compounds

journal homepage: www.elsevier.com/locate/jallcom

Crystal structures and magnetic properties of iron (III)-based phosphates: $Na_4NiFe(PO_4)_3$ and $Na_2Ni_2Fe(PO_4)_3$

Rachid Essehli[a,*], Brahim El Bali[a], Said Benmokhtar[b], Khalid Bouziane[c], Bouchaib Manoun[d], Mouner Ahmed Abdalslam[e], Helmut Ehrenberg[f]

[a] Laboratory of Mineral Solid and Analytical Chemistry "LCSMA", Department of Chemistry, Faculty of Sciences, University Mohamed I, Po. Box 717, 60000 Oujda, Morocco
[b] LCMS, Laboratoire de Chimie des Matériaux Solides, Département de chimie, Faculté des Sciences Ben M'SIK, Casablanca, Morocco
[c] Physics Department, College of Science, Sultan Qaboos University, PO Box 36, Postal Code 123 Al Khod, Sultanate of Oman
[d] Laboratoire de Physico-Chimie des Matériaux, Département de Chimie, FST Errachidia, University Moulay Ismail, B.P. 509 Boutalamine, Errachidia, Morocco
[e] Materials Science, Technical University Darmstadt, Darmstadt, Germany
[f] IFW Dresden, Helmholtzstr. 20, D-01069 Dresden, Germany

ARTICLE INFO

Article history:
Received 21 June 2010
Received in revised form 25 August 2010
Accepted 27 August 2010
Available online 27 October 2010

Keywords:
Synthesis
Crystal structure
Nasicon
Alluaudite
Magnetism
Hyperfine interaction

ABSTRACT

Crystal structures from two new phosphates $Na_4NiFe(PO_4)_3$ (**I**) and $Na_2Ni_2Fe(PO_4)_3$ (**II**) have been determined by single crystal X-ray diffraction analysis. Compound (I) crystallizes in a rhombohedral system (S. G: *R*-3*c*, $Z=6$, $a=8.7350(9)$ Å, $c=21.643(4)$ Å, $R_1=0.041$, $wR_2=0.120$). Compound (**II**) crystallizes in a monoclinic system (S. G: *C*2/*c*, $Z=4$, $a=11.729(7)$ Å, $b=12.433(5)$ Å, $c=6.431(2)$ Å, $\beta=113.66(4)^\circ$, $R_1=0.043$, $wR_2=0.111$). The three-dimensional structure of (**I**) is closely related to the Nasicon structural type, consisting of corner sharing $[(Ni/Fe)O_6]$ octahedra and $[PO_4]$ tetrahedra forming $[NiFe(PO_4)_3]^{4+}$ units which align in chains along the *c*-axis. The Na^+ cations fill up trigonal antiprismatic sites within these chains. The crystal structure of (**II**) belongs to the alluaudite type. Its open framework results from $[Ni_2O_{10}]$ units of edge-sharing $[NiO_6]$ octahedra, which alternate with $[FeO_6]$ octahedra that form infinite chains. Coordination of these chains yields two distinct tunnels in which site Na^+.

The magnetization data of compound (I) reveal antiferromagnetic (AFM) interactions by the onset of deviations from a Curie–Weiss behaviour at low temperature as confirmed by Mössbauer measurements performed at 4.2 K. The corresponding temperature dependence of the reciprocal susceptibility χ^{-1} follows a typical Curie–Weiss behaviour for $T>105$ K. A canted AFM state is proposed for compound (II) below 46 K with a field-induced magnetic transition at $H\approx 19$ kOe, revealed in the hysteresis loop measured at 5 K. This transition is most probably associated with a spin-flop transition.

1. Introduction

Inorganic phosphates cover a large class of diverse materials whose applications include: catalysts, solid electrolytes for batteries [1–7], linear and non-linear optical components [8–11] and laser materials [12,13]. However, the study of phosphates has become more popular particularly after the development of the compounds containing $[A_2(XO_4)_3]$ fragments in the underlying framework. Common structure types are Garnet, Nasicon, Alluaudite, $[Sc_2(WO_4)_3]$ and Langbeinite (Figs. 1–4). In general, these structures have the same type of framework, but with different types of holes, cavities, tunnels for cations accommodation. Physical and chemical properties of all these types of compounds depend strongly on their crystal structure. Nasicon and Alluaudite structure types of interest for this study and therefore described in more detail.

1.1. Nasicon compounds

The basic structure of these compounds was first described by Hagman and Kierkegaard [14]. These phosphates have been widely studied in many fields, because of their various properties such as conductivity, low expansion coefficients and catalytic activity [15–19]. They have fascinated much awareness in recent past, as they facilitate a large scope for preparing number of materials with variation in their constituent metal ions and composition [20–24]. These materials have the general formula $B_pA_nA'_m(PO_4)_3$ where B is a monovalent cation Na^+, Ag^+, Cu^+, H^+, H_3O^+, NH_4^+, or a divalent one such as Mn^{2+}, Fe^{2+}, Co^{2+}, Ni^{2+} or Cu^{2+}, while *A* and *A*′ can be filled with tri-, tetra- or pentavalent transition metal ions. Thus the structure can be tailored by substituting at *B*, *A*, and/or *A*′ sites which gives rise to a large number of com-

* Corresponding author.
E-mail addresses: rachid_essehli@yahoo.fr, essehli_rachid@yahoo.fr (R. Essehli).

0925-8388/$ – see front matter © 2010 Elsevier B.V. All rights reserved.
doi:10.1016/j.jallcom.2010.08.159

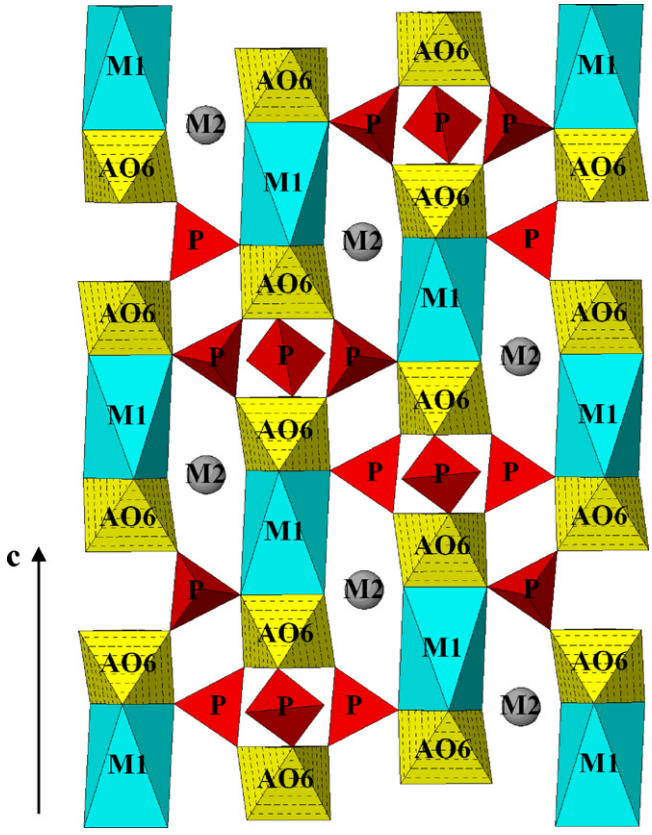

Fig. 1. The structure of Nasicon showing the M(1) (type 1) and M(2) sites (type 2).

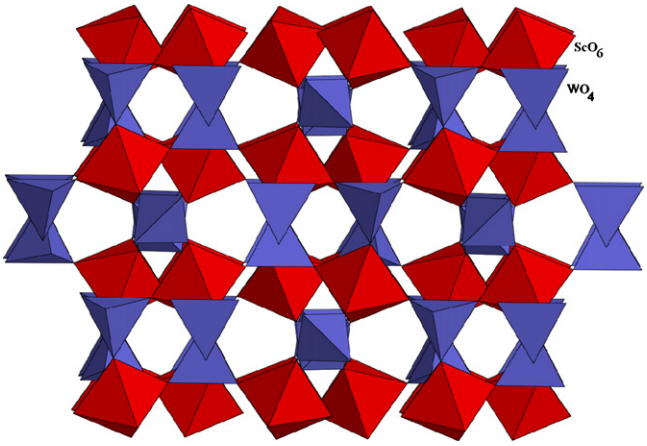

Fig. 3. The polyhedral unit cell structure of $Sc_2(WO_4)_3$ as viewed down the *a*-axis.

pounds for comparative studies. The crystal structure consists of a three-dimensional network built up from corners sharing of $[PO_4]$ tetrahedra and $[AO_6]$ ($[A'O_6]$) octahedra. Every apex of $[AO_6]$ octahedron belongs to one $[PO_4]$ tetrahedron. The two distinct interstitial voids generated within the network are known as M(1) and M(2) sites. The M(1) site is a trigonally distorted octahedron formed by the triangular faces of two $[AO_6]$ octahedra along the *c*-axis of the hexagonal cell. The M(2) sites are located in the large cavities and have an eight-fold coordination. There is one atom on a M(1) site per three atoms on a M(2) site according to the formula unit $M(1)_xM(2)_yA_n(PO_4)_3$ with $0 \le x \le 1$ and $0 \le y \le 3$. Most of the members of Nasicon type compounds so far known in the literature are described in rhombohedral $R\bar{3}c$, $R\bar{3}$ or $R32$ space groups with typical unit cell dimensions $a \sim 8$ Å and $c \sim 22$ Å, but cell

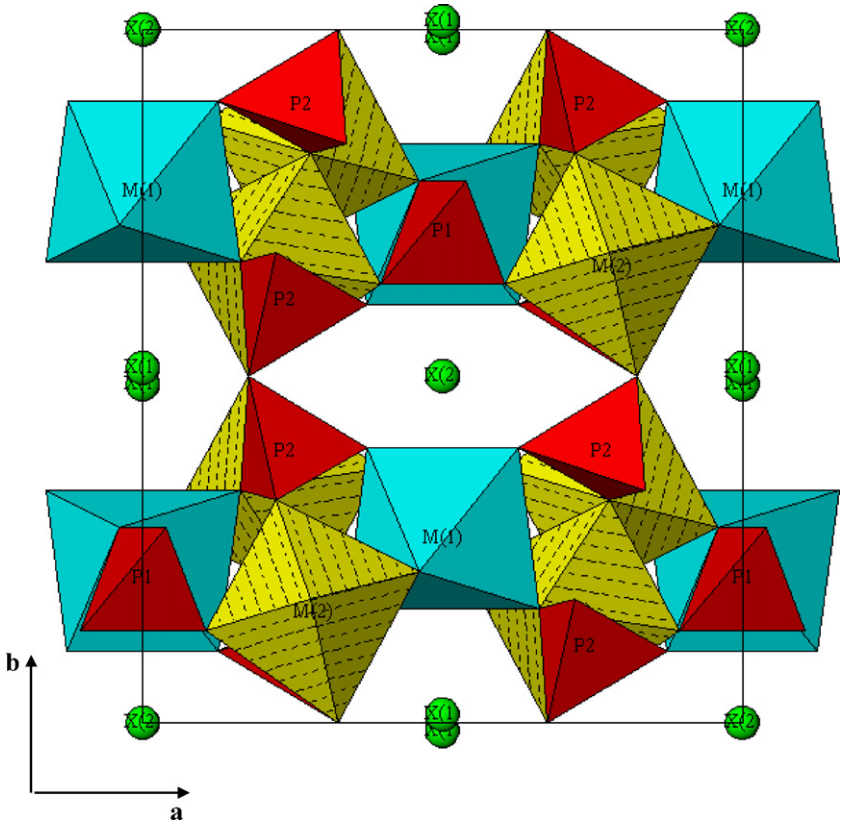

Fig. 2. Polyhedral representation of the alluaudite unit cell showing the open-framework channel structure propagating along [0 0 1].

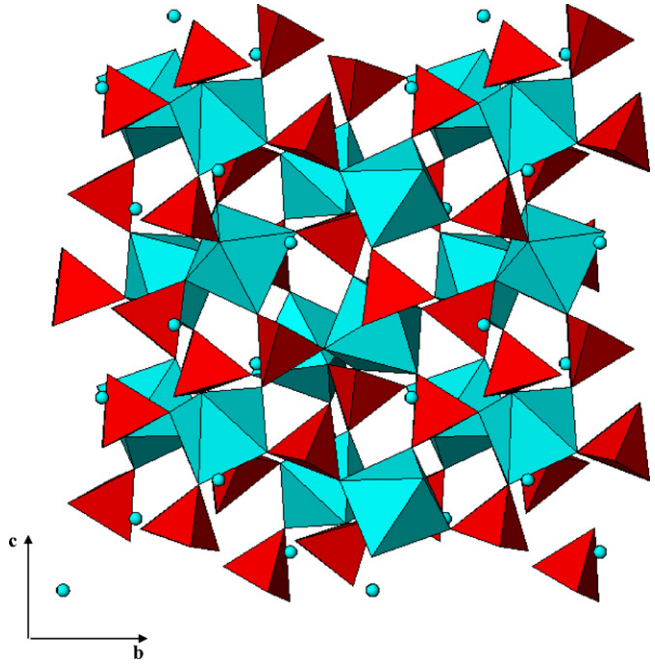

Fig. 4. Polyhedral model of the langbeinite structure projected down the *a*-axis.

distortions leading to a monoclinic symmetry have been also reported [25,26].

1.2. Alluaudite compounds

The alluaudite-type compounds have been extensively studied in the context of corrosion inhibition [27], passivation of metal surfaces [28], and heterogeneous catalysis [29]. The crystal structure was first described by Moore [30] who studied a single crystal of $Na_{0.625}Li_{0.025}Ca_{0.125}Mn_{1.125}Mg_{0.05}Fe_{1.975}(PO_4)_3$ from the Buranga pegmatite originating from Rwanda. The crystal structure of this compound was assigned to a monoclinic system with *C*2/*c* space group and a general structural formula $X(2)X(1)M(1)M(2)_2(PO_4)_3$ ($Z=4$), where X are large cation polyhedral, M are distorted octahedral, and P the tetrahedral centers [30]. The cations are distributed among the different crystallo-

Table 1
Summary of crystal data, intensity measurement, and structure refinement for $Na_4NiFe(PO_4)_3$ (I) and $Na_2Ni_2Fe(PO_4)_3$ (II).

	$Na_4NiFe(PO_4)_3$ (I)	$Na_2Ni_2Fe(PO_4)_3$ (II)
Structural formula	$Na_4NiFe(PO_4)_3$ (I)	$Na_2Ni_2Fe(PO_4)_3$ (II)
Molecular weight	491.43	598.38
Crystal system	Hexagonal	Monoclinic
Space group	$R-3c$ (167)	$C2/c$ (15)
Cell dimension	$a=8.7350(9)$ Å $b=8.7350(9)$ Å $c=21.643(4)$ Å	$a=11.729(7)$ Å $b=12.433(5)$ Å $c=6.431(2)$ Å $\beta=113.66(4)$
Cell volume	1430.1(3)	858.9(6)
Z	6	4
Density (g cm^{-1})	3.424	4.627
$F(0\,0\,0)$	1434	1128
θ range (°)	4.63–31.96	2.50–31.25
Index range	$-11\le h\le 0$, $0\le k\le 12$, $0\le l\le 30$	$-16\le h\le 13$, $-18\le k\le 17$, $-9\le l\le 9$
Data collection temperature (K)	293(2)	293(2)
Number of parameters	35	95
Goodness of fit on F^2	1.225	1.241
Final R indices [$I>2\sigma(I)$]	$R_1=0.0414$, $wR_2=0.1201$	$R_1=0.0434$, $wR_2=0.1111$
Extinction coefficient	0.0010(5)	0.0016(3)

Table 2
Atomic coordinates for $Na_4NiFe(PO_4)_3$ (I) and $Na_2Ni_2Fe(PO_4)_3$ (II).

Atom	Site	*x*	*y*	*z*	Ueq
Fe	12c	**0.0000**	**0.0000**	**0.1482(4)**	**0.0091(3)**
Ni	12c	**0.0000**	**0.0000**	**0.1482(4)**	**0.0091(3)**
P	18e	**−0.3333**	**−0.3740(1)**	**0.0833**	**0.0079(3)**
Na(1)	6b	**0.0000**	**0.0000**	**0.0000**	**0.071(3)**
Na(2)	18e	**−0.3333**	**−0.0301(5)**	**0.0833**	**0.0545(1)**
O(1)	36f	**0.1819(5)**	**0.2060(5)**	**0.1924(1)**	**0.0235(7)**
O(2)	36f	**0.1900(4)**	**0.0215(4)**	**0.0874(1)**	**0.0132(6)**
Ni	8f	**0.2164(7)**	**0.3422(6)**	**0.1281(11)**	**0.0099(2)**
Fe	4e	**0.0000**	**0.2332(8)**	**0.2500**	**0.0067(2)**
P(1)	4e	**0.0000**	**0.20890(15)**	**−0.2500**	**0.0070(3)**
P(2)	8f	**0.2639(12)**	**0.1097(10)**	**0.3776(2)**	**0.0066(3)**
Na(1)	4a	**0.0000**	**0.0000**	**0.0000**	**0.0148(7)**
Na(2)	4e	**0.5000**	**−0.0118(5)**	**0.7500**	**0.0467(1)**
O(1)	8f	**0.0393(4)**	**0.2809(3)**	**−0.0356(6)**	**0.0107(7)**
O(2)	8f	**0.3250(4)**	**−0.0007(3)**	**0.3875(7)**	**0.0111(7)**
O(3)	8f	**0.2788(4)**	**0.1787(3)**	**0.1874(6)**	**0.0097(7)**
O(4)	8f	**0.3385(4)**	**0.1653(3)**	**0.6104(6)**	**0.0088(7)**
O(5)	8f	**0.1044(4)**	**0.1330(3)**	**−0.2446(7)**	**0.0116(7)**
O(6)	8f	**0.1259(4)**	**0.1028(3)**	**0.3311(7)**	**0.0131(7)**

Table 3
Anisotropic displacement parameters (Å$^2\times 10^3$).

Atom	U_{11}	U_{22}	U_{33}	U_{23}	U_{13}	U_{12}
Fe	9.3(3)	9.3(3)	8.9(4)	0.000	0.000	4.63(17)
Ni	9.3(3)	9.3(3)	8.9(4)	0.000	0.000	4.63(17)
P	5.9(5)	5.5(4)	12.3(6)	−1.2(2)	−2.5(4)	3.0(3)
Na(1)	99(5)	99(5)	16(3)	0.000	0.000	49(2)
Na(2)	26.8(18)	30.1(14)	106(4)	−9.1(11)	−18(2)	13.4(9)
O(1)	18.7(15)	20.8(15)	28.7(16)	−14.7(13)	−12.1(12)	8.2(13)
O(2)	8.0(12)	15.5(13)	16.9(12)	1.4(10)	3.3(9)	6.6(10)
Ni	13.0(3)	9.1(3)	7.4(3)	−0.6(2)	3.8(2)	−0.4(2)
Fe	7.7(4)	7.6(5)	4.7(4)	0.000	2.3(3)	0.000
P(1)	**0.0084(7)**	**0.0088(8)**	**0.0026(7)**	**0.000**	**0.0008(6)**	**0.000**
P(2)	**10.3(6)**	**5.9(5)**	**3.0(5)**	**0.2(4)**	**2.0(4)**	**0.1(4)**
Na(1)	27.7(17)	5.3(13)	4.1(13)	1.4(10)	−1.1(12)	1.7(12)
Na(2)	32(2)	62(4)	35(3)	0.000	2(2)	0.000
O(1)	10.9(16)	15.3(18)	4.4(15)	−0.6(13)	1.6(13)	2.2(14)
O(2)	17.3(18)	5.9(15)	9.7(16)	1.0(13)	5.0(14)	2.9(13)
O(3)	12.9(17)	11.5(17)	4.3(15)	0.7(13)	3.0(13)	0.4(13)
O(4)	15.3(17)	8.4(16)	0.9(14)	0.3(12)	1.3(13)	−0.8(13)
O(5)	12.1(17)	10.3(16)	11.4(17)	−4.4(13)	3.6(14)	1.2(13)
O(6)	11.1(17)	13.8(18)	13.8(18)	0.6(15)	4.4(14)	−0.1(14)

The anistropic displacement factor exponent takes the form: $-2\pi[h^2a^{*2}U_{11}+\cdots+2hka^*b^*U_{12}$.

Table 4
Comparison of the parameters of the phosphates $Na_4NiFe(PO_4)_3$ (I) with those of $Na_4AA'(PO_4)_3$.

$Na_4AA'(PO_4)_3$	$r(AA')$ Å	a_h (Å)	c_h (Å)	V_h (Å^3)	References
$Na_4NiFe(PO_4)_3$	0667	8735	21,643	1430	This work
$Na_4FeFe(PO_4)_3$	0712	8,9543	21,280	1477	[36]
$Na_4NiCr(PO_4)_3$	0652	8789	21,481	1437	[37]
$Na_4MgCr(PO_4)_3$	0667	8831	21,500	1452	[38]
$Na_4CoCr(PO_4)_3$	0680	8840	21,541	1458	[39]
$Na_4NaTi(PO_4)_3$	0813	9061	21,734	1545	[40]
$Na_4NaZr(PO_4)_3$	0870	9152	21,844	1584	[41]

graphic sites in dependence on their ionic radii. Accordingly, the large X(2) site contains Na and vacancies; X(1) contains Na, Mn, and Ca; M(1) contains Mn and Fe^{2+}; and the small M(2) site hosts Fe^{3+}, Fe^{2+}, Mn, Mg, and Li. Because Mn dominates on the M(1) site, and Fe^{2+} and Fe^{3+} dominate on the M(2) site, Moore proposed thus the ideal formula $Na_2MnFe^{2+}Fe^{3+}(PO_4)_3$, from which the majority of natural alluaudites can be derived [30]. The structure of alluaudite consists of kinked chains of edge-sharing octahedra stacked parallel to (1 0 1). These chains are formed by a succession of M(2) octahedral pairs linked by highly distorted M(1) octahedra. Equivalent chains are connected in the *b* direction by phosphates groups to form sheets oriented perpendicular to [0 1 0]. These interconnected sheets produce tunnels parallel to the *c*-axis, which contain the distorted cubic X(1) site and the four-coordinated X(2) site. Over the past decade, many arsenates, molybdates, phosphates, tungstates and vanadates, with the Alluaudite structure have been synthesized. The structural investigations of these synthetic compounds showed the existence of new crystallographic sites localized in the channels of the structure, on positions which are different from those of X(1) and X(2). In order to take these new crystallographic sites into account, Hatert et al. [31] proposed the new general formula $[A(2)A(2)'][A(1)A(1)'A(1)''_2]M(1)M(2)_2(PO_4)_3$ for alluaudite-type compounds. In this formula, A(1) and A(2)′ correspond to X(1) and X(2), respectively.

There are different ways to prepare new kinetically stable solid compounds at low temperature. The most common techniques are hydrothermal synthesis and chemical vapour transport or the use of molten salts (or flux growth) to dissolve reactants at relatively low temperature. In the present paper, we report hereby on the synthesis, using a flux method, of two new monophosphates [$Na_4NiFe(PO_4)_3$ (I) and $Na_2Ni_2Fe(PO_4)_3$ (II)] in the ternary system Na_3PO_4–$Ni_3(PO_4)_2$–$FePO_4$. Their crystallographic structure

Table 5
Selected bond lengths (Å) and angles for $Na_4NiFe(PO_4)_3$ (I).

Fe–O(1)	3 × 1.955(3)	O(2)–Na(1)–O(2)	6 × 112.77(10)
Fe–O(2)	3 × 2.050(3)	O(2)–Na(1)–O(2)	3 × 180.00(18)
P–O(1)	2 × 1.526(3)	O(2)–Na(2)–O(2)	162.0(2)
P–O(2)	2 × 1.533(3)	O(2)–Na(2)–O(2)	129.52(15)
Na(2)–O(1)	2 × 2.600(4)	O(2)–Na(2)–O(2)	2 × 68.43(14)
Na(2)–O(1)	2 × 2.855(5)	O(2)–Na(2)–O(2)	61.13(16)
Na(1)–O(2)	6 × 2.462(3)	O(2)–Na(2)–O(1	2 × 115.47(10)
Na(2)–O(2)	2 × 2.390(3)	O(2)–Na(2)–O(1)	2 × 68.31(10)
Na(2)–O(2)	2 × 2.458(5)	O(2)–Na(2)–O(1)	2 × 67.17(12)
O(1)–Fe–O(1)	3 × 98.05(16)	O(2)–Na(2)–O(1)	2 × 93.11(15)
O(1)–Fe–O(2)	3 × 169.48(15)	O(2)–Na(2)–O(1)	68.31(10)
O(1)–Fe–O(2)	3 × 88.68(14)	O(1)–Na(2)–O(1)	157.6(2)
O(1)–Fe–O(2)	3 × 88.35(14)	O(2)–Na(2)–O(1)	2 × 109.92(16)
O(1)–Fe–O(2)	3 × 88.94(14)	O(2)–Na(2)–O(1)	2 × 54.70(10)
O(1)– P–O(1)	111.2(3)	O(2)–Na(2)–O(1)	2 × 115.20(10)
O(1)–P–O(2)	2 × 112.11(18)	O(2)–Na(2)–O(1)	2 × 151.97(11)
O(1)–P–O(2)	2 × 106.11(18)	O(1)–Na(2)–O(1)	2 × 111.41(14)
O(1)–P–O(2)	109.3(2)	O(1)–Na(2)–O(1)	2 × 85.95(8)
O(2)–Na(1)–O(2)	6 × 67.23(10)	O(1)–Na(2)–O(1)	81.10(19)

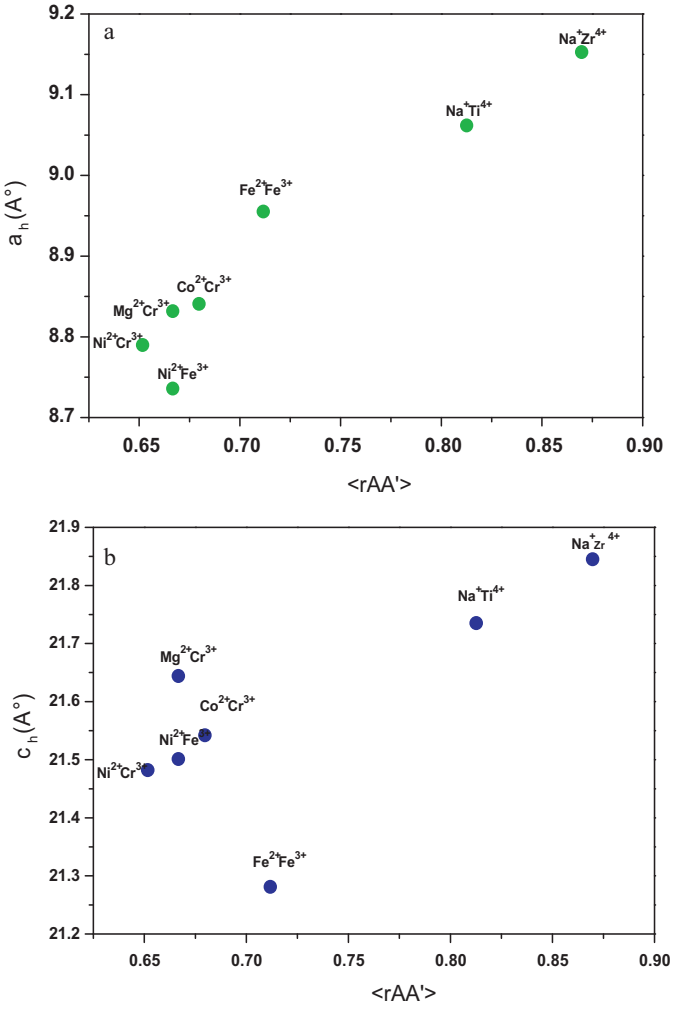

Fig. 5. Cell parameter variations as a function of *r* for $Na_4AA'(PO_4)_3$ (AA′ = CrMg, CrCo, FeFe, NiFe, TiNa, ZrNa).

are described in detail and their magnetic and hyperfine interaction properties are also reported.

2. Experimental

2.1. Synthesis

The crystals grown used in the present study were obtained in a synthesis aiming at the hypothetic diphosphate "$Na_3Ni_2Fe(PO_4)_2(P_2O_7)$" in flux of sodium dimolybdate $Na_2Mo_2O_7$. A starting mixture of $Fe(NO_3)_3{\cdot}9H_2O$, $Ni(NO_3)_2{\cdot}3H_2O$, $(NH_4)_2HPO_4$, Na_2CO_3 and MoO_3 was mixed in the appropriate proportions to obtain the nominal composition and then ground. The mixture was placed in a platinum crucible and then subjected to several steps of heat treatment. Firstly, the mixture was heated at 200 °C for 6 h and then at 500 °C for 24 h to decompose H_2O, NH_3 and CO_2. Single crystals were prepared by melting the resulting powder at 1150 ± 20 °C for 15 h and then cooled down progressively to 500 °C at rate of 3 °C/h and faster after switching off the furnace to reach room temperature. A mixture of yellow and yellow-green crystals was obtained.

2.2. Structure determination

Brown single crystals with dimension 0.40 mm × 0.18 mm × 0.08 mm for $Na_4NiFe(PO_4)_3$ (I) and 0.20 mm^3 × 0.25 mm^3 × 0.15 mm^3 for $Na_2Ni_2Fe(PO_4)_3$ (II) were selected. The data for both crystals were recorded at room temperature on an Oxford Diffraction Xcalibur (TM) diffractometer, operating at 40 kV and 30 mA and with a graphite monochromator (Mo–Kα radiation, λ = 0.71073 Å). The cell parameters were refined from the complete data sets. Absorption corrections were computed by the Gaussian method taking into consideration the shape and the size of the crystals.

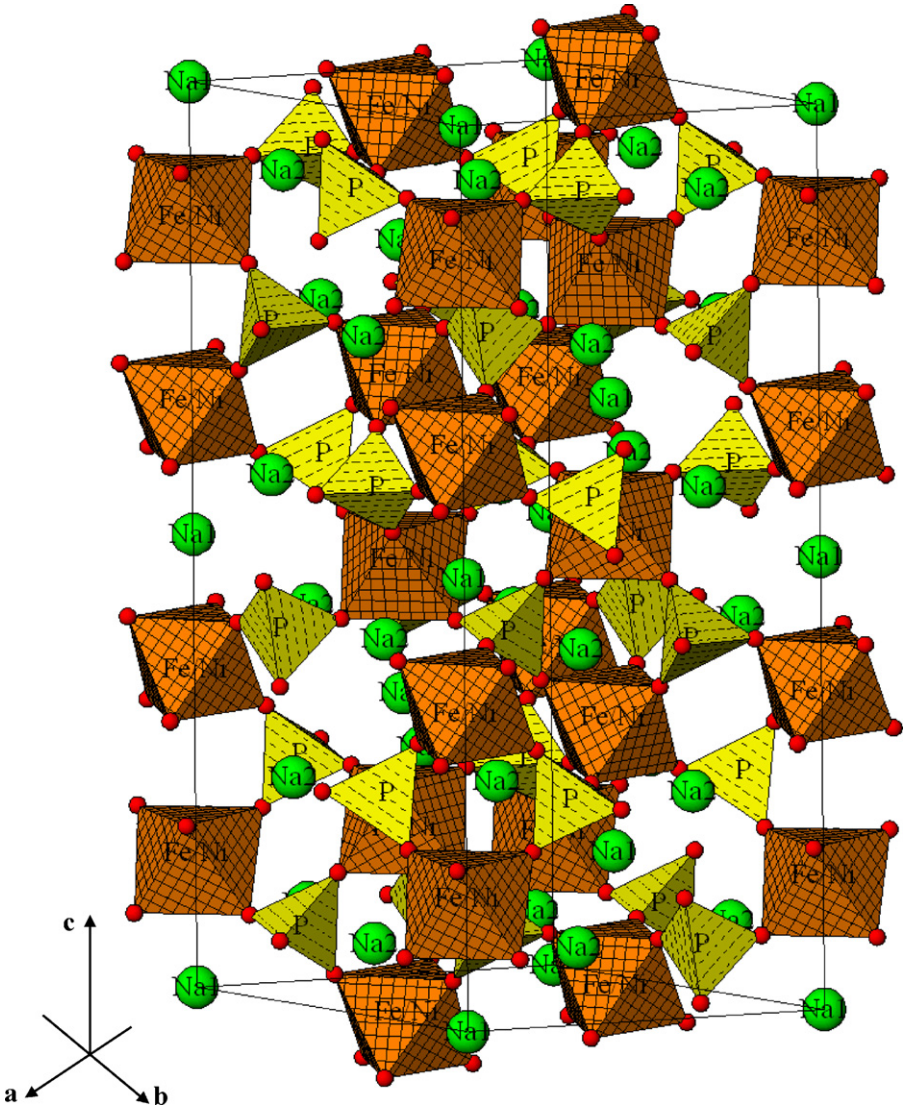

Fig. 6. A polyhedral view of framework of $Na_4NiFe(PO_4)_3$ (I) as projected in the (b and c) plane.

$Na_4NiFe(PO_4)_3$ (I) crystallizes in rhombohedral symmetry with the following lattice parameters $a = 8.7350(9)$ Å and $c = 21.643(4)$ Å in the hexagonal setting. A first refinement in space group $R3$ converged to a satisfactory model with $R_1 = 0.0521$, but a check of these structural data with the program ADDSYM immediately allowed to identify additional symmetry elements, thus confirming the $R-3c$ (167) space group.

$Na_2Ni_2Fe(PO_4)_3$ (II) crystallizes in monoclinic symmetry with the lattice parameters $a = 11.729(7)$ Å, $b = 12.433(5)$ Å, $c = 6.431(2)$ Å and $\beta = 113.66(4)^\circ$. The systematic absences $h+k=2n+1$, $l=2n+1$ and $h=2n+1$ for $h\,0\,1$ and $k=2n+1$ for $0\,k\,0$ are consistent with the $C2/c$ (1 5) space group.

Experimental details, refinement parameters and crystal data for both compounds are summarized in Table 1.

Both structures were solved by the heavy atom method. The full matrix least-squares refinements of the atomic parameters were performed on the F-values weighted by $1/\sigma(F)2$ using the SHELX-97 suite [32,33] in the WinGX framework [34]. They lead to $R_1 = 0.041$ and $R_w = 0.120$ for $Na_4NiFe(PO_4)_3$ (**I**) and to $R_1 = 0.043$ and 0.111 for $Na_2Ni_2Fe(PO_4)_3$ (**II**). Atomic coordinates in both compounds are reported in Tables 2 and 3. Further details of the crystals structure investigations are reported elsewhere [35].

2.3. Magnetic characterization

The magnetization was measured with a DMS 1660 vibrating sample magnetometer (VSM) in a magnetic field up to 13.5 kOe. The sample was first cooled down to 105 K under an applied field of 13.5 kOe, and then the measurements were performed when warming the sample up to 303 K under the same magnetic field. The VSM was calibrated using pure nickel (Ms = 54.9 emu/g).

3. Result and discussion

3.1. Description of the structures

3.1.1. $Na_4NiFe(PO_4)_3$ (I)

Compound (**I**) crystallizes in the trigonal system R-3c, it belongs to the Nasicon family. Table 4 compares the parameters of $Na_4NiFe(PO_4)_3$ (I) with those of $Na_4AA'(PO_4)_3$ (AA′ = CrMg, CrCo, NiFe, TiNa, ZrNa). Fig. 5a and b shows the variation of the crystallographic parameters of these Nasicon-type phosphates in which the sum of the A and A′ cations charges on the octahedral site is +5. The linear variations of these parameters versus the mean A cation radius (rAA') are consistent with the atomic distribution for the $Na_4NiFe(PO_4)_3$ structure in which the Ni^{2+} and Fe^{3+}cations occupy the A sites randomly. Fig. 5a and b shows that both the a_h and c_h parameters increase when r_{AA} "cations radius" increases. As the M(1) and M(2) sites are fully occupied by Na(1), we conclude that the a_h and c_h parameters are functions of the A^{n+} ion size, c_h parameter also increases with the strength of the Na^+ (M(1))– A^{n+} electrostatic repulsion.

3.1.1.1. Ni/Fe distribution. The distribution of Ni/Fe atoms is discussed in more detail. The structure is based on a three-dimensional

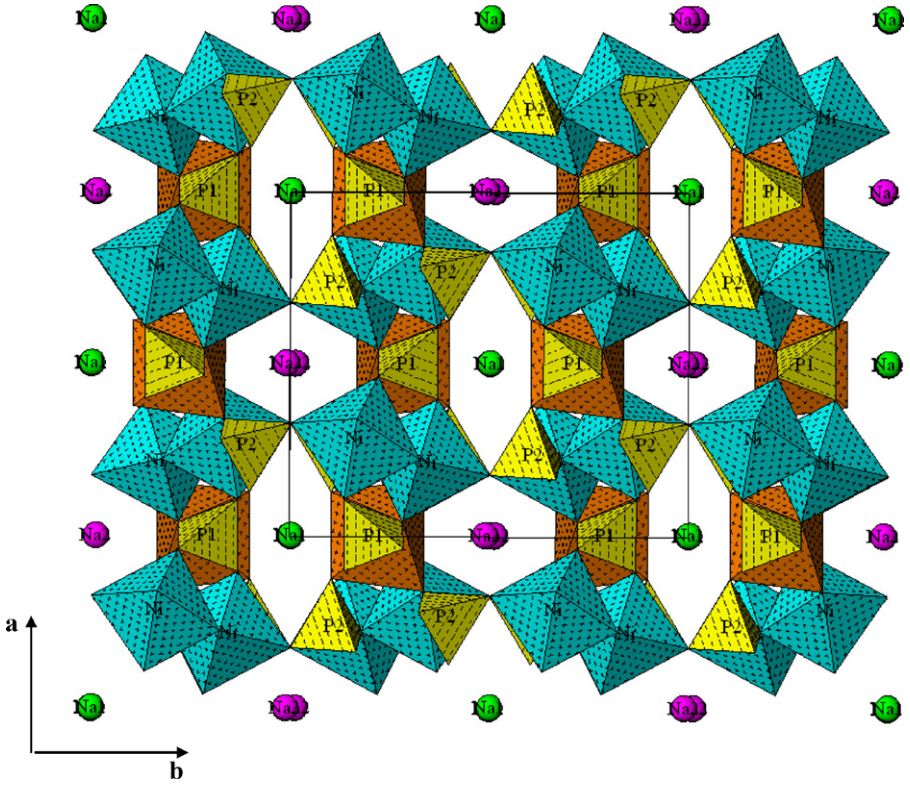

Fig. 7. A perspective view of the $Na_2Ni_2Fe(PO_4)_3$ structure along the [0 0 1] direction.

framework of [PO_4] tetrahedra and [(Fe/Ni)O_6] octahedra sharing corners (Fig. 6). Fe^{3+} and Ni^{2+} ions occupy statistically the 12c sites. Ni/Fe atoms are displaced from the center of the octahedron due to the Na^+–Fe^{3+}/Ni^{2+} repulsions. The O(1) and O(2) sites play distinct roles. Indeed, O(2) constitutes the octahedral M(1) cavity between adjacent Fe/Ni$(PO_4)_3$ lantern units along [0 0 1], while O(1) constitutes the empty "internal" cavity located between the two [FeO_6] octahedra of the Fe/Ni$(PO_4)_3$ lantern unit (Fig. 6). Consequently the Fe^{3+}/Ni^{2+}–O(2) distance is 2.053(3) Å, neighboring the sodium Na(1), is slightly greater than the Fe^{3+}/Ni^{2+}–O(1) distance 1.955(3) Å (Table 5). On the other hand, the Fe^{3+}–Fe^{3+} distance through the Na(1) site along [0 0 1] increases from 6.414(3) Å in $Na_4NiFe(PO_4)_3$ (I) to 6.487 Å in γ-$Na_3Fe_2(PO_4)_3$. The average Fe^{3+}/Ni^{2+}–O distances 2.002 Å are slightly smaller than the values calculated from the ionic radii (2.075 Å) [42]. The O–(Fe^{3+}/Ni^{2+})–O angles vary between 83.35(12)° and 169.48(15)°. The angles implying the shortest bonds are superior to those involving the longest ones as a consequence of the O–O repulsions which are stronger for O(1)–O(1) than for O(1)–O(2) and O(2)–O(2). The Fe^{3+}/Ni^{2+}–Fe^{3+}/Ni^{2+} distance within the lantern unit along [0 0 1] (4.406(5) Å) is lower to the Fe^{3+}–Fe^{3+} distance in γ-$Na_3Fe_2(PO_4)_3$ (4.417(2) Å) [43], due to the cationic repulsions between ions on 12c sites. These repulsions are stronger in $Na_3Fe_2(PO_4)_3$ (charge of iron is 3) than in $Na_4NiFe(PO_4)_3$ (I) (mean charge of Fe^{3+}/Ni^{2+} = 2.5).

The P–O distances values (1.526(3)–1.533(3) Å) are close to those typically found in Nasicon-like phosphates [(1.533(6)–1.538(6) Å and (1.508(2)–1.541(2) Å)] in $Na_4Fe^{2+}Fe^{3+}(PO_4)_3$ and γ-$Na_3Fe^{3+}{}_2(PO_4)_3$, respectively] [36,43]. O–P–O angles vary from 106.11(8) to 112.11(8) [(106.9(3)–112.1(3) Å)] in $Na_4Fe^{2+}Fe^{3+}(PO_4)_3$.

Na^+ cations occupy partially the M(1) and M(2) sites. The Na(1) atoms occupy the center of the M(1) site. Na(1)–O(2) distance (2.463(2) Å (Table 5) is close to 2.40(2(5) Å in $Na_4Fe^{2+}Fe^{3+}(PO_4)_3$, which in turn is close to the calculated one (2.42 Å) from the ionic radii [42] (2.500(1) Å in γ-$Na_3Fe_2(PO_4)_3$). The Na(2) atoms, located in the M(2) site, are surrounded by eight oxygen atoms, the Na(2)–O distances vary from 2.390(3) to 2.855(5) Å induces close values for the Na(2)–O distances for $Na_4Fe^{2+}Fe^{3+}(PO_4)_3$ and γ-$Na_3Fe_2(PO_4)_3$, respectively.

3.1.2. *$Na_2Ni_2Fe(PO_4)_3$ (II)*

The general structure of $Na_2Ni_2Fe(PO_4)_3$ is isostructural to the alluaudite-type. A perspective view of this structure along the [0 0 1] direction is illustrated in Fig. 7. The open framework is built up from a complex arrangement of [NiO_6] and [FeO_6] octahedral and [PO_4] tetrahedra. The essential building units of the structure are Ni_2O_{10} units resulting from two edge-sharing [NiO_6] octahedra. Neighbouring [Ni_2O_{10}] are connected by the [FeO_6] octahedra through edge-sharing that form infinite chains with a stacking sequence of Ni–Ni–Fe and passing through the unit cell in the direction [1 0 $\bar{1}$]. Linkage of these chains being ensured by the [PO_4] tetrahedra via corners and the resulting three-dimensional framework delimits two kinds of tunnels in the [0 0 1] direction. These tunnels are occupied by the Na^+ ions.

Ni^{2+} is coordinated to six oxygen ions, every [NiO_6] polyhedron is connected to another [NiO_6] by common edge (O(3)–O(3)) and form a binuclear unit [Ni_2O_{10}] (Fig. 8) with Ni–Ni distance of 3.105 Å. The other corners O(1), O(2), O(4) and O(5) are connected to [PO_4] tetrahedra. The angle O(3)–Ni–O(3) is 85.07(15)° and the Ni–O distances range from 1.952(4) Å to 2.143(4) Å (Table 6). This dispersion evidences a fair distortion of the [NiO_6] octahedron due to the edge-sharing.

The iron coordination has a very distorted octahedral geometry, as evidenced by the Fe–O bond distances between 2.112(4) and 2.150(4) Å. The O–Fe–O bond angles vary between 74.88(14)° and 164.78(15)° (Table 6). This distortion is probably due to the rigidity of [PO_4] units surrounding the Fe atom.

There are two crystallographically distinct sites, occupied by P^{5+} cations, both tetrahedrally coordinated. P–O bond distances for each [PO_4] tetrahedron range from 1.527(4) to 1.560(4) Å and

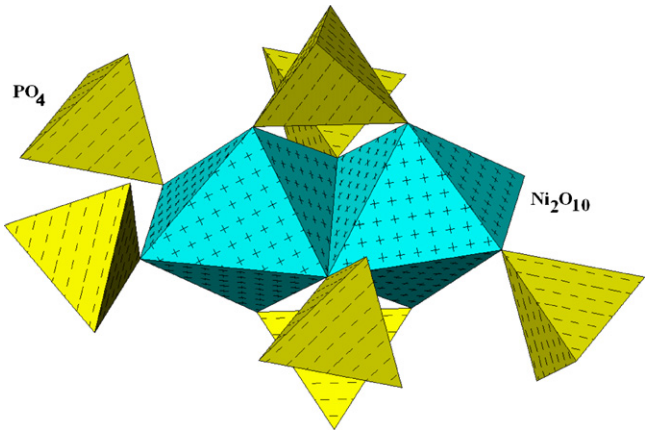

Fig. 8. Dimer block Ni_2O_{10} and PO_4 tetrahedra in $Na_2Ni_2Fe(PO_4)_3$.

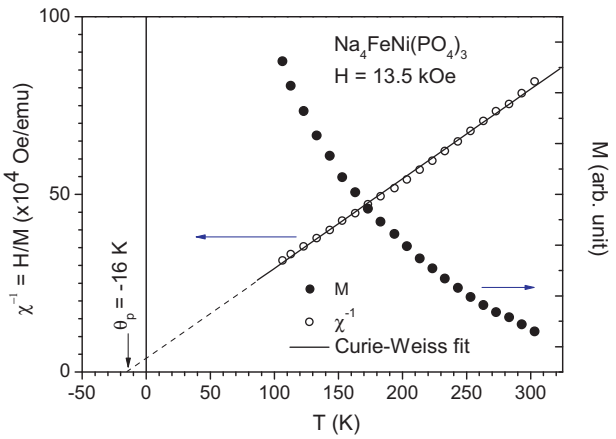

Fig. 9. The magnetic susceptibility $\chi^{-1} = H/M$ versus temperature and the corresponding magnetization measured under an applied field $H = 13.5$ kOe.

Table 6
Selected bond lengths (Å) and angles for $Na_2Ni_2Fe(PO_4)_3$ (II).

Ni O(5)	1.952(4)	O(6)–Fe–O(4)	86.33(15)
Ni O(2)	2.004(4)	O(6)–Fe–O(4)	164.78(15)
Ni O(4)	2.030(4)	O(4)–Fe–O(4)	108.2(2)
Ni O(1)	2.062(4)	O(1)–Fe–O(4)	86.39(15)
Ni O(3)	2.069(4)	O(1)–Fe–O(4)	74.88(14)
Ni O(3)	2.143(4)	O(5)–P(1)–O(5)	104.1(3)
Fe O(6)	2.112(4)	O(5)–P(1)–O(1)	112.6(2)
Fe O(6)	2.114(4)	O(5)–P(1)–O(1)	2 × 109.0(2)
Fe O(4)	2 × 2.148(4)	O(5)–P(1)–O(1)	112.7(2)
Fe O(1)	2.149(4)	O(1)–P(1)–O(1)	109.5(3)
Fe O(4)	2.150(4)	O(6)–P(2)–O(2)	113.3(2)
P(1) O(5)	1.534(4)	O(6)–P(2)–O(3)	108.8(2)
P(1) O(5)	1.536(4)	O(2)–P(2)–O(3)	109.0(2)
P(1) O(1)	1.551(4)	O(6)–P(2)–O(4)	110.8(2)
P(1) O(1)	1.551(4)	O(2)–P(2)–O(4)	106.5(2)
P(2)O(6)	1.527(4)	O(3)–P(2)–O(4)	108.2(2)
P(2) O(2)	1.537(4)	O(5)–Na(1)–O(5)	180.0
P(2) O(3)	1.560(4)	O(5)–Na(1)–O(6)	2 × 102.17(14)
P(2) O(4)	1.560(4)	O(5)–Na(1)–O(6)	2 × 77.83(14)
Na(1) O(5)	2 × 2.305(4)	O(6)–Na(1)–O(6)	180.00(17)
Na(1) O(6)	2 × 2.414(4)	O(5)–Na(1)–O(6)	2 × 72.97(14)
Na(1) O(6)	2 × 2.504(4)	O(5)–Na(1)–O(6)	2 × 107.03(14)
Na(1) O(5)	2 × 2.874(4)	O(6)–Na(1)–O(6)	2 × 66.80(17)
Na(2) O(2)	2 × 2.414(4)	O(6)–Na(1)–O(6)	2 × 113.20(17)
Na(2) O(2)	2 × 2.544(4)	O(6)–Na(1)–O(6)	180.00(13)
Na(2)O(4)	2.806(7)	O(5)–Na(1)–O(5)	2 × 54.41(17)
Na(2)O(4)	2.809(7)	O(5)–Na(1)–O(5)	2 × 125.59(17)
Na(2)O(1)	2.871(7)	O(6)–Na(1)–O(5)	2 × 86.19(13)
Na(2)O(1)	2.872(7)	O(6)–Na(1)–O(5)	2 × 93.81(13)
O(5)–Ni–O(2)	2 × 93.82(17)	O(6)–Na(1)–O(5)	2 × 113.50(12)
O(5)–Ni–O(4)	109.91(16)	O(6)–Na(1)–O(5)	2 × 66.50(12)
O(2)–Ni–O(4)	86.39(16)	O(5)–Na(1)–O(5)	180.00(18)
O(5)–Ni–O(1)	164.47(16)	O(2)–Na(2)–O(2)	173.4(4)
O(2)–Ni–O(1)	99.28(17)	O(2)–Na(2)–O(2)	80.82(13)
O(4)–Ni–O(1)	79.39(15)	O(2)–Na(2)–O(2)	2 × 98.78(13)
O(5)–Ni–O(3)	86.99(16)	O(2)–Na(2)–O(2)	80.81(13)
O(2)–Ni–O(3)	100.02(16)	O(2)–Na(2)–O(2)	173.0(3)
O(4)–Ni–O(3)	161.62(15)	O(2)–Na(2)–O(4)	2 × 56.16(14)
O(1)–Ni–O(3)	82.57(15)	O(2)–Na(2)–O(4)	2 × 117.8(2)
O(5)–Ni–O(3)	81.03(16)	O(2)–Na(2)–O(4)	61.92(14)
O(2)–Ni–O(3)	172.62(15)	O(2)–Na(2)–O(4)	2 × 112.0(2)
O(4) Ni O(3)	90.38(15)	O(2)–Na(2)–O(4)	61.81(14)
O(1) Ni O(3)	86.62(16)	O(4)–Na(2)–O(4)	76.6(2)
O(3) Ni O(3)	85.07(15)	O(2)–Na(2)–O(1)	71.14(16)
O(6) Fe O(6)	79.7(2)	O(2)–Na(2)–O(1)	2 × 115.2(2)
O(6) Fe O(4)	164.76(15)	O(2)–Na(2)–O(1)	102.9(2)
O(6) Fe O(4)	86.30(15)	O(2)–Na(2)–O(1)	83.43(16)
O(6) Fe O(1)	111.62(16)	O(4)–Na(2)–O(1)	126.34(12)
O(6) Fe O(1)	93.09(16)	O(4)–Na(2)–O(1)	2 × 144.65(12)
O(4) Fe O(1)	74.95(14)	O(2)–Na(2)–O(1)	71.20(16)
O(6) Fe O(1)	93.15(16)	O(2)–Na(2)–O(1)	83.28(17)
O(6) Fe O(1)	111.70(16)	O(2)–Na(2)–O(1)	103.1(2)
O(4) Fe O(1)	86.35(15)	O(4)–Na(2)–O(1)	126.39(12)
O(1)Fe O(1)	148.0(2)	O(1)–Na(2)–O(1)	52.33(19)

O–P–O bond angles range from 104.1(3) to 113.3(2)°. These results are in a good agreement with those usually observed in anhydrous monophosphates [44,45]. The $[P(1)O_4]$ tetrahedron connects two chains by sharing each pair of its oxygen O(1) and O(5) with one chain. The $[P(2)O_4]$ tetrahedron links three adjacent chains and thus two of its oxygen atoms belong to the same chain.

The three-dimensional framework of (II) leads to two types of tunnels at $x = 1/2$; $y = 0$ and $x = 0$; $y = 0$ which are occupied by the sodium atoms Na(1) and Na(2), respectively. Taking into account cation – oxygen distances below 3.0 Å, the Na(1) and Na(2) sites are both surrounded by eight oxygen atoms. Their environments approximate a very distorted rhombohedron and a very distorted cube, respectively. Each of the $[Na(1)O_8]$ and $[Na(2)O_8]$ polyhedra form infinite chains stacked parallel to the [0 0 1] direction by face-sharing.

The crystal structure of $Na_2Ni_2Fe(PO_4)_3$ is closely related to the alluaudite type structure of the mixed valent iron phosphates: $Na_2Fe^{II}{}_2Fe^{III}(PO_4)_3$ [36], with one main difference being the presence of separated $[Fe_2O_{10}]$ units of edge-sharing $[FeO_6]$ octahedra. In terms of the $X(2)X(1)M(1)M(2)_2(PO_4)_3$ general formula of the alluaudite, the M(1) and M(2) environments have both an octahedral geometry. These octahedra share their edges with each other to form infinite chains running along the [1 0 1] direction. In the structure of $Na_2Ni_2Fe(PO_4)_3$ (II), the M(2) site is occupied by Ni while M(1) contains only Fe atoms. The chains characterizing the alluaudite structure are then built up from $[Ni_2O_{10}]$ units alterning with $[FeO_6]$ octahedra.

4. Magnetic properties

4.1. $Na_4FeNi(PO_4)_3$

Fig. 9 shows the temperature dependence of the inverse magnetic susceptibility χ^{-1} and the corresponding magnetization measured at $H = 13.5$ kOe for $Na_4FeNi(PO_4)_3$. The $\chi^{-1}(T)$ curve obeys a Curie–Weiss law down to 100 K, with negative T-intercept, namely the Weiss constant $\theta_p = -16$ K indicating antiferromagnetic exchange interactions. Such interactions can be expected for the underlying crystal structure, in which Fe^{3+} and Ni^{2+} ions occupy statistically the 12c sites and the $[(Fe/Ni)O_6]$ octahedra could be coupled via a superexchange mechanism through O–P–O bridges from $[PO_4]$ tetrahedral, resulting in magnetic ordering as confirmed by Mössbauer spectroscopy discussed below. The room temperature Mössbauer spectrum of $Na_4FeNi(PO_4)_3$ (Fig. 10a) was fitted with one Lorentz-type symmetric quadrupole doublet, in agreement with the existence of one crystallographic Fe site. Note that

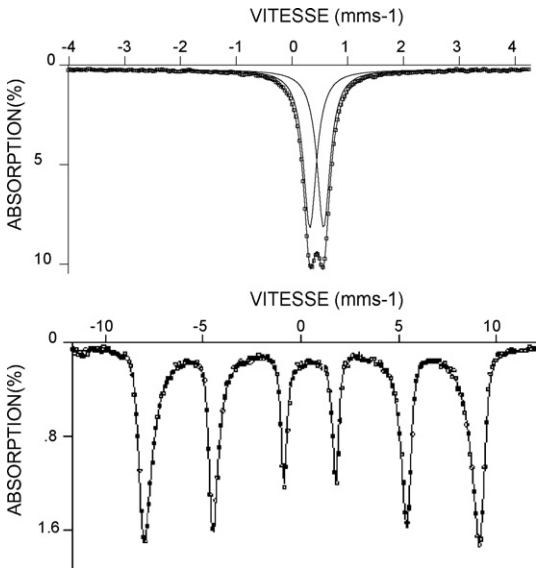

Fig. 10. Mössbauer spectra of $Na_4NiFe(PO_4)_3$ (a) $T = 293$ K, (b) $T = 4.2$ K.

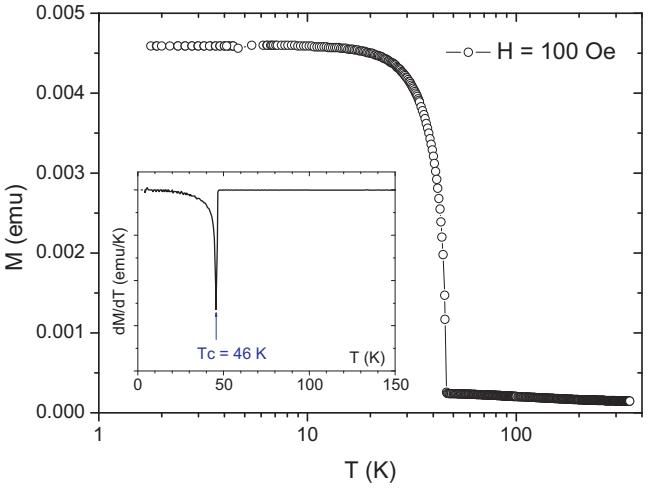

Fig. 12. Temperature dependence of magnetization M(T) measured at 100 Oe when warming the sample. Note the log-scale of temperature axis for clarity.

the intensity of each doublet was constrained to be equal as well as the width of the peaks (I, Γ). The isomer shifts (δ) clearly indicate the high-spin state of Fe^{3+} ions in an octahedral oxygen crystal field, typically close to 0.48 mm/s for Fe^{3+} in sixfold coordination as reported by Menil [46]. The observed value of 0.42 mm/s is in agreement with highly ionic Fe–O bonds due to the inductive effect by the phosphate polyanions as established by Gleitzer [47]. The quadrupole splitting $\Gamma = 0.27$ mm/s reflects a highly distorted octahedral configuration of Fe^{3+}. The Mössbauer spectrum of $Na_4NiFe(PO_4)_3$ measured at 4.2 K is shown in Fig. 10b. It has been fitted with four magnetic sextets of equal relative areas and widths of peaks. The hyperfine fields are rather similar (56.0 and 54.4 T) and typical for a high-spin Fe^{3+} ion close to saturation. The value of the isomer shifts (0.54 mm/s) is in agreement with the second-order Doppler shift. These results confirm the expected antiferromagnetic ground state due to superexchange coupling between Fe(Ni) ions.

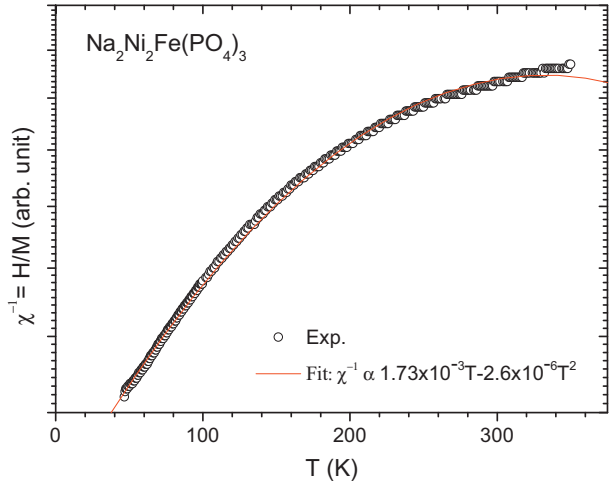

Fig. 11. Temperature dependence of magnetic susceptibility $\chi = H/M$ showing almost a Curie–Weiss behaviour above Curie temperature $T_c = 46$ K (the coefficient of the second order on temperature is three order of magnitude less than that of the first order).

4.2. $Na_2Ni_2Fe(PO_4)_3$

The results of magnetic susceptibility measurements in the temperature range from 1.7 to 350 K are plotted in Fig. 11. In the range 50–300 K, the inverse magnetic susceptibility follows ($r = 0.9999$) the Curie–Weiss law $\chi^{-1} = 9.5(1) + 0.05(1)T$, C being 20 cm^3K/mol. The fitted parameters together with the measured effective magnetic moments ($\mu_{effexp} = (8C)^{1/2}$ is 12.64 μ_B, even higher than the spin-only contributions from Ni^{2+} ($3d^8$) and Fe^{3+}($3d^5$) [$\mu_{effcal} = 11.56\,\mu_B$]. The magnetic behaviour for $Na_2Ni_2Fe(PO_4)_3$ presents interesting features. Fig. 12 shows the corresponding temperature dependence of the magnetization M(T) measured at 100 Oe revealing a ferromagnetic component below

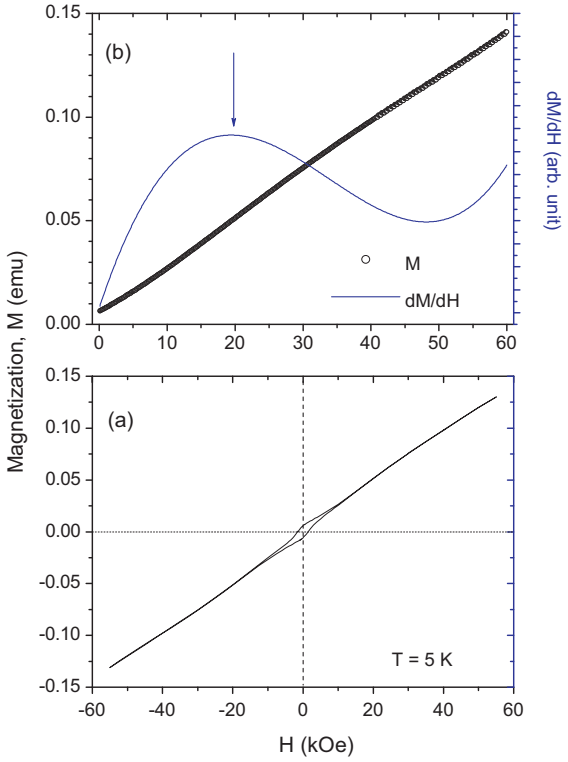

Fig. 13. (a) Hysteresis loop at 5 K; and (b) the corresponding field derivative of the positive saturation magnetization branch.

the Curie temperature of about $T_c = 46$ K as clearly determined from the temperature derivative of magnetization. However, the magnetization above T_c does not vanish but shows a progressive decrease. The corresponding reciprocal susceptibility χ^{-1} as a function of temperature above T_c is displayed in Fig. 11. The χ^{-1} data can be essentially attributed to a Curie–Weiss behaviour ($\chi^{-1} = (1/C)(T-\theta_p)$, although some weak magnetic order persists above T_c as indicated by the curvature of χ^{-1} versus T.A hysteresis loop M(H) at 5 K (up to 55 kOe) is shown in Fig. 13a. The observed remnant magnetization and the coercivity $Hc = 1.5$ kOe support the existence of a FM phase (see Fig. 13b). The large slope in the high-field region reveals that only small components of the magnetic moments are ferromagnetically aligned. This means either weak ferromagnetism in a canted antiferromagnetic structure of ferrimagnetism. A careful inspection of M(H) curve indicates a change in the slope with field, most pronounced in the field-derivative of magnetization $(\partial M/\partial H)_T$ as shown in Fig. 13b. A field-induced transition might be indicated from the reflection point at about 30 kOe in $(\partial M/\partial H)_T$ and would be compatible with a canted AFM state as reported for other phosphate-based systems [48,49].

5. Conclusions

Crystals from two new monophosphates have been prepared using a flux method. Their crystal structures have been determined. $Na_4NiFe(PO_4)_3$ is characterized by a 3D framework, Ni^{2+} and Fe^{3+} occupy statistically the same crystallographic site, magnetically coupled by supersuperexchange via O–P–O bridges from [PO_4] orthophosphate groups. In the allaudite-type phosphate $Na_2Ni_2Fe(PO_4)_3$ [NiO_6] and [FeO_6] octahedral share edges to form trimers in the structure. The magnetic properties have been discussed, based on magnetization studies and Mössbauer spectroscopy.

Acknowledgments

Authors would like to thank Dr Dusek [Institute of Physics, Praha, Czeck Republic] for his continuous collaboration.

References

[1] (a) R. Essehli, B. El Bali, H. Ehrenberg, I. Svoboda, N. Bramnik, H. Fuess, Mater. Res. Bull. 44 (2009) 817–821;
(b) R. Essehli, B. El Bali, H. Ehrenberg, I. Svoboda, K. Nikolowski, N. Bramnik, H. Fuess, in: 24th European Crystallographic Meeting, ECM24, Marrakech, 2007 (MS21 P07), Proc. Acta Cryst. A 63 (2007) s212.
[2] I.M. Nagpure, K.N. Shinde, Kumar Vinay, O.M. Ntwaeaborwa, S.J. Dhoble, H.C. Swart, J. Alloys Compd. 492 (1–2) (2010) 384–388.
[3] A. Salah, P. Jozwiak, J. Garbarczyk, K. Benkhouja, K. Zaghib, F. Gendron, C.M. Julien, J. Power Sources 140 (2005) 370–375.
[4] F. Mauvy, E. Siebert, A. Ahmad, J. Eur. Ceram. Soc. 19 (1999) 917–919.
[5] W. Ling, R.V. Kumar, Solid State Ionics 158 (2003) 309–315.
[6] T. Jiang, G. Chen, Ang Li, C. Wang, Y. Wei, J. Alloys Compd. 478 (1–2) (2009) 604–607.
[7] S.Y. Chung, J.T. Bloking, Y.M. Chiang, Nat. Mater. 2 (2002) 123–128.
[8] J.-K. Sun, F.-Q. Huang, Y.-M. Wang, Z.-C. Shan, Z.-Q. Liu, M.-L. Liu, Y.-J. Xia, K.-Q. Li, J. Alloys Compd. 469 (2009) 327–331.
[9] I. Juwiler, A. Arie, A. Skliar, G. Rosenman, Opt. Lett. 24 (1999) 1236–1238.
[10] J. Hellstrom, V. Pasiskevicius, F. Laurell, H. Karlsson, Opt. Lett. 24 (1999) 1233–1235.
[11] J. Zhang, J. Wang, B. Ge, Y. Liu, X. Hu, R.I. Boughton, J. Cryst. Growth 267 (2004) 517–521.
[12] G.D. Stucky, M.L.F. Phillips, T.E. Gier, Chem. Mater. 1 (1989) 492–509.
[13] J.D. Bierlein, H. Vanheerzeele, J. Opt. Soc. Am. B 6 (1989) 622–633.
[14] L.O. Hagman, P. Kierkegaard, Acta Chem. Scand. 22 (1968) 1822–1832.
[15] J.S. Kim, P.E. Jeon, J.C. Choi, H.L. Park, Solid State Commun. 133 (2005) 187–190.
[16] N. Anantharamulu, K. Koteswara Rao, M. Vithal, G. Prasad, J. Alloys Compd. 479 (2009) 684–691.
[17] J.K. Feng, L. Lu, M.O. Lai, J. Alloys Compd. 501 (2010) 255–258.
[18] R. Roy, D.K. Agrawal, J. Alamo, R.A. Roy, Mater. Res. Bull. 19 (1984) 471–477.
[19] Y. Brik, M. Kacimi, F. Bozon-Verduraz, M. Ziyad, Micropour. Mater. Mesopor. Mater. 43 (2001) 103–112.
[20] R. Essehli, B. El Bali, S. Benmokhtar, K. Fejfarová, M. Dusek, Mater. Res. Bull. (2009) 1502–1510.
[21] N. Anantharamulu, R. Velchuri, T. Sarojini, K. Madhavi, G. Prasad, M. Vithal, Indian J. Eng. Mater. Sci. (2009) 347–354.
[22] N. Anantharamulu, K. Koteswara Rao, G. Prasad, M. Vithal, J. Alloys Compd. 479 (2009) 684–691.
[23] T. Masui, K. Koyabu, S. Tamura, N. Imanaka, J. Alloys Compd. 418 (2006) 73–76.
[24] A. El Bouari, A. El Jazouli, S. Benmokhtar, P. Gravereau, A. Wattiaux, J. Alloys Compd. 503 (2010) 480–484.
[25] J.P. Boilot, J.P. Salanié, G. Desplanches, D. Le Potier, Mater. Res. Bull. 14 (1979) 1469–1477.
[26] U. von Alpen, M.F. Bell, W. Wichelhaus, Mater. Res. Bull. 14 (1979) 1317–1322.
[27] W. Meisel, H.J. Guttmann, P. Gütlich, Corros. Sci. 23 (1983) 1373–1379.
[28] M.B. Korzenski, G.L. Schimek, J.W. Kolis, G.J. Long, J. Solid State Chem. 139 (1998) 152–160.
[29] J.B. Moffat, Catal. Rev. Sci. Eng. 18 (1978) 199–258.
[30] P.B. Moore, Am. Miner. 56 (1971) 1955–1975.
[31] F. Hatert, P. Keller, F. Lissner, D. Antenucci, A.-M. Fransolet, Eur. J. Mineral 12 (2000) 847–857.
[32] G.M. Sheldrick, SHELXS-97––A Program for Automatic Solution of Crystal Structures, University of Goettingen, Goettingen, Germany, 1997.
[33] G.M. Sheldrick, SHELXL-97––A Program for Crystal Structure Refinement, University of Goettingen, Goettingen, 1997.
[34] L.J. Farrujia, J. Appl. Crystallogr. 32 (1999) 837–838.
[35] Fachinformationszentrum Karlsruhe, 76344 Eggenstein Leopoldshafen, Germany (fax: +49 7247 808 666; E-mail: crysdata@fiz.karlsruhe.de) on quoting the depository numbers CSD 421434 for $Na_4NiFe(PO_4)_3$ (I) and CSD 421435 for $Na_2Ni_2Fe(PO_4)_3$ (II).
[36] Hatert Frederic, Acta Cryst. E 65 (2009) i30.
[37] B. Manoun, A. El Jazouli, S. Krimi, A. Lachgar, Powder Diffraction 19 (2004) 162–164.
[38] C. Delmas, F. Cherkaoui, P. Hagenmuller, Mater. Res. Bull. 21 (1986) 469–477.
[39] H. El Kinani, DESA de Chimie, University Hassan II, Casablanca, Morocco, 2000.
[40] S. Krimi, I. Mansouri, A. El Jazouli, J.P. Chaminade, P. Gravereau, G. Le Flem, J. Solid State Chem. 105 (1993) 561–566.
[41] J.P. Boilot, G. Collin, R. Comes, Solid State Chem. 50 (1983) 829–833.
[42] R.D. Shannon, Acta Crystallogr. A 32 (1976) 751–767.
[43] C. Masquelier, C. Wurm, J. Rodrguez-Carvajal, J. Gaubicher, L. Nazar, Chem. Mater. 12 (2) (2000) 525–532.
[44] P.G. Nagornoy, A.A. Kapshuck, N.V. Stuss, N.S. Slobodyanik, Zh. Neorg. Khim. 34 (1989) 3030.
[45] S. Benmokhtar, A. El Jazouli, A. Aatiq, J.P. Chaminade, P. Gravereau, A. Wattiaux, L. Fournès, J.C. Grenier, J. Solid State Chem. 180 (2007) 2004–2012.
[46] F. Menil, J. Phys. Chem. Solids 46 (7) (1985) 763.
[47] C. Gleitzer, Eur. J. Solid State Inorg. Chem. 28 (1991) 77–91.
[48] He Zhangzhen, S.C. Chen, C.S. Lue, Cheng Wendan, Ueda Yutaka, Phys. Rev. B78 (2008) 1–4, 212410/.
[49] He Zhangzhen, Ueda Yutaka, Itoh Mitsuru, Solid State Commun. 141 (2007) 22–24.